Direct Computation of Higher Order Mode Components from Successively Linearized Geometrically Nonlinear Beam Theory

Markus Ritter*
DLR - Institute of Aeroelasticity, Göttingen, Germany

The extended modal approach is a simplified nonlinear method for the steady and unsteady computation of geometrically nonlinear structural deflections that was developed for loads and flight dynamics analyses of highly flexible aircraft. Compared to the classical modal approach, which is based on the superposition of normal modes, the extensions include higher order stiffness terms and higher order mode components to account for nonlinearities both in the load displacement relationships (cubic stiffness terms) as well as in the geometrically nonlinear displacement field (large deflections and rotations of structural components). These extensions make the method particularly suitable for aeroelastic applications involving highly flexible structures and nonlinearities due to nonconservative loads. In this work, a new approach for the calculation of the higher order mode components is proposed which uses the nonlinear relationships between strains (or curvatures) and displacements from a geometrically nonlinear beam theory. The idea is take the curvatures of a particular structural mode and to integrate them using successively linearized compatibility equations to compute the higher order mode components. In his way, the higher order mode components are directly obtained, and the costly pre-processing step with a series of nonlinear static simulations is circumvented.

I. Motivation and Introduction

Some classes of aircraft are characterized by highly flexible airframes exhibiting pronounced structural deflections in steady and maneuvering flight. High altitude, long endurance (HALE) type of aircraft as well as next generation jet transports with high aspect ratio wings are prominent examples. Design criteria such as reduction of the induced drag almost inevitably lead to wings of high slenderness and aspect ratio. Analyzing and designing highly flexible aircraft puts great demands on the methods and tools employed. Multidisciplinary analysis taking into account aerodynamics, flight mechanics, and structural dynamics is indispensable where nonlinearities due to large rigid body and structural deflections are inherent in each of these disciplines and must be taken into account from the beginning. For the structural part, only few methods exist so far for the calculation of general aircraft structures undergoing large deformations. Commercial Finite Element solver are mostly limited to clamped structures in their nonlinear solution capabilities. On the other hand, sophisticated methods incorporating nonlinear rigid body and elastic motions have been developed for beam type structural models only. A recently developed method (the extended modal approach) is aiming to fill this gap by extension of the classical modal approach to account for its major limitations [1–4]. Nonlinear force-displacement relations (generalized quadratic and cubic stiffness terms) and a geometrically nonlinear displacement field, which is represented by quadratic, cubic, and fourth-order mode components, are accounted for as well as a load dependent stiffness function, similar to the tangential stiffness matrix used in nonlinear finite element analyses. Quadratic mode components were successfully applied by Segalman and Dohrmann to model rotating structures undergoing large displacements [5], van Zyl used them for T-Tail flutter analyses [6, 7]. Despite the advantages, one issue with the extended modal approach is the calculation of the higher order mode components, which is done by a series of static nonlinear solutions using a commercial FE solver and specific force fields for the particular structure. The higher order mode components are then computed from the static nonlinear responses by polynomial fitting. This process is rather complex and requires a careful selection of the magnitudes of the structural deformations in the nonlinear identification step [3].

This work proposes a new approach for the calculation of the higher order mode components for beam-like structures as well as structural models that have a beam-like topology (such models are typically obtained by static condensation – Guyan reduction – of detailed, complex finite element models). The new approach is based on strain-displacement relationships used in geometrically nonlinear beam theory. Following the calculation of curvatures (from the applied loads) along the beam or the structure, the nonlinear finite rotations of the reference line of the beam is computed which

*Group leader in the Loads Analysis and Aeroelastic Design department of DLR, Markus.Ritter@dlr.de

yields the orientations of the cross sections. For simplicity, the orientations of the cross sections are parametrized by Euler angles. The displacements of the beam in the global frame of reference are computed by another set of nonlinear compatibility equations which are formulated as first-order differential equations. The two sets of nonlinear compatibility equations include particular trigonometric functions. These functions can be approximated (linearized) by Taylor series expansions. Applying successive series expansions of the trigonometric functions in which linear, quadratic, and cubic terms are kept, the curvatures along the beam reference line can be integrated to obtain linear, quadratic, and cubic rotations and displacements. These displacements of different order can be used to directly compute the higher order mode components of a beam for a particular mode shape. The curvatures, which are required for this process, belong to a particular mode shape, they can be calculated by differentiation of the nodal rotations of that mode. Two test cases are used in this work to demonstrate the proposed approach, the well known 16m beam configuration, and a slender composite wingbox.

II. Theoretical Background of the Extended Modal Approach

A. Theoretical Derivation

The derivation of the extended modal approach is given in detail in Ref. [3], the final governing equations are presented in the following. Compared to the classical modal approach, the extended modal approach is based on a nonlinear force-displacement relationship by quadratic and cubic stiffness terms, as given in the following nonlinear governing equation in pseudo-generalized coordinates:

$$ {}^{p}G_1^i \, q_i + {}^{p}G_2^{ij} \, q_i q_j + {}^{p}G_3^{ijk} \, q_i q_j q_k = Q^p \quad (p = 1, \ldots, m) \tag{1} $$

Where the ${}^{p}G_n$ tensors denote the generalized stiffnesses and $\boldsymbol{q}$ the vector of generalized coordinates. The stiffness tensors G_n are determined by polynomial fitting or numerical differentiation [3].

The second extension is the reconstruction of a geometrically nonlinear displacement field based on higher-order mode components (here up to fourth order). Usually, the structure's eigenvectors realize the linear transformation from generalized to physical coordinates. For the extended modal approach this linear relationship is extended, the mode shape ${}^{p}\boldsymbol{\Phi}$ includes components of higher-order and becomes a function of the generalized coordinates:

$$ {}^{p}\boldsymbol{\Phi} = {}^{p}\boldsymbol{\Phi}_0 + {}^{p}\boldsymbol{\Phi}_1^i \, q_i + {}^{p}\boldsymbol{\Phi}_2^{ij} \, q_i q_j + {}^{p}\boldsymbol{\Phi}_3^{ijk} \, q_i q_j q_k \tag{2} $$

The term ${}^{p}\boldsymbol{\Phi}_0$ can be seen as the equivalent of the structure's normal modes.

Considering Eq.(1), the forcing term of the structure's governing equation, the generalized force Q^p, is normally calculated by the product of the transposed eigenvector matrix and the forces on the structure's nodes, $\boldsymbol{f}$. Here, the quadratic mode components ${}^{p}\boldsymbol{\Phi}_1^i$ extend the generalized forces to yield a dependency of Q^p on the amplitude of deformation [6, 7]:

$$ Q^p = {}^{p}\boldsymbol{\Phi}_0{}^{T} \boldsymbol{f} + {}^{p}\boldsymbol{\Phi}_1^{i\,T} \boldsymbol{f} \, q_i \tag{3} $$

Combining Eq.(1) and (3) yields:

$$ ({}^{p}G_1^i - {}^{p}\boldsymbol{\Phi}_1^{i\,T} \boldsymbol{f}) \, q_i + {}^{p}G_2^{ij} \, q_i \, q_j + {}^{p}G_3^{ijk} \, q_i \, q_j \, q_k = {}^{p}\boldsymbol{\Phi}_0{}^{T} \boldsymbol{f} \tag{4} $$

Eq.(4) is the static governing equation of the extended modal approach. Compared to the classical modal approach, the ${}^{p}G_1^i$ term is amended by the product of the transpose of the quadratic mode component matrix and the force field. This additional stiffness parameter is of importance especially in aeroelastic applications [3]. Subsequent to the solution of the governing equation for the generalized coordinates $\boldsymbol{q}$, the nodal deformation field in Cartesian coordinates is approximated by the higher order mode components:

$$ \mathbf{u}(\boldsymbol{q}) = {}^{p}\boldsymbol{\Phi}_0 \, q_p + {}^{p}\boldsymbol{\Phi}_1^i \, q_p q_i + {}^{p}\boldsymbol{\Phi}_2^{ij} \, q_p q_i q_j + {}^{p}\boldsymbol{\Phi}_3^{ijk} \, q_p q_i q_j q_k \tag{5} $$

B. Original Approach for the Calculation of the Higher Order Mode Components

A crucial issue of the extended modal approach is the determination of the linear and the higher-order stiffness terms and mode components, which must be done in a preprocessing step. Depending on the structural model considered,

different approaches exist for the determination of the nonlinear stiffness terms. Methods that calculate the higher-order terms by a series of nonlinear, static FE solutions are in general favorable since static solutions are computationally cheap [8]. This approach was followed over the last years and a commercial FE program (MSC Nastran) is used which provides the strain energy and, of course, the nonlinear deformation field as part of the solution. The basic idea for the calculation of the higher order stiffness terms and mode components is the application of special force fields on the structure and the computation of nonlinear solutions with these force fields. The force fields are defined such that the resulting displacement field (as computed by a linear or nonlinear FE analysis) yields a displacement field which is exactly a structural mode shape. Assuming the natural (in vacuo) eigenvalues and corresponding eigenvectors of the structure are available and using one selected eigenvector/mode shape, such a force field (denoted as $\boldsymbol{F}^i$) can be defined as:

$$\mathbf{F}_i = \mathbf{K}\,\boldsymbol{\phi}^i\,q_i \quad , \tag{6}$$

where $\mathbf{K}$ denotes the linear stiffness matrix of the structure, q_i a scaling factor (for now), and $\boldsymbol{\phi}^i$ denotes the column vector of one of the natural eigenvectors of the structure. Applying this force field in a nonlinear FE simulation results in nodal displacements u_i which are a function of the scaling parameter q_i. Using a comparatively small value for q_i – which in turn yields small deformations – results in a deformation field that qualitatively equals the mode shape $\boldsymbol{\phi}^i$. Increasing the value of q_i in the nonlinear simulation at some point results in a deformation field that shows significant differences to the linear deformation field. This becomes obvious if for example the first bending mode shape is applied to $\boldsymbol{\phi}^i$. The linear part of the deformation field consists of pure transverse displacements, whereas for larger values of q_i in-plane deformations significantly emerge. The strain energies and displacement fields which are obtained from nonlinear static analyses (using MSC Nastran) for different scaling factors q_i can be fitted by higher order polynomials. The linear, quadratic, cubic, and fourth-order coefficients of the polynomials correspond to the higher order stiffness terms and mode components defined in Eq.(1) and Eq.(2) [3].

C. Exemplary Application of the Extended Modal Approach to a Beam Structure

To demonstrate particular features of the extended modal approach we consider a cantilever beam with a length of 16 meters that resembles a generic, slender aircraft wing and is subject to different kinds of loadings in a geometrically nonlinear structural analysis [3]. The beam is discretized by 32 finite beam elements (here, Nastran *CBEAM* beam elements were used) and 33 nodes, all properties of the FE model are listed in the Appendix of [3]. The moments of inertia of the cross section of the beam vary quadratically along the axis of the beam. This setup was chosen to obtain bending deformations with almost constant curvature as the beam is subjected to forces with elliptic distribution (similar to aerodynamic forces). Discrete mass elements were used to tune the dynamic structural behavior. The layout of the model is shown in Fig. 1.

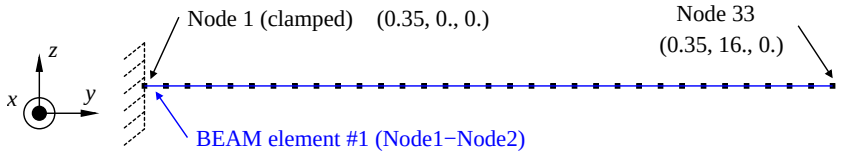

Fig. 1 FE model of the 16 m beam test case composed of 33 nodes and 32 elements, clamping at Node 1.

Applying a constant force field in the y and in the z direction depicts significant differences between the nonlinear and the linear results. Deformations of the beam structure are shown in Fig. 2 for a constant force field applied at each node in the negative y and in the positive z direction in six steps from 50 N to 300 N, respectively. Good agreement between the results of the extended modal approach and the nonlinear FE solution is achieved. For this type of loading, the force component in the y direction takes no effect in the linear solution. The reason is that the force is applied onto the undeformed structure, and the component in the y direction leads to a very small deformation (compression) in the axial direction of the beam only. By contrast, the extended modal approach is able to account for the forces acting in the axial direction because of the the linear stiffness term which becomes a function of the applied force field, as defined by Eq.(4).

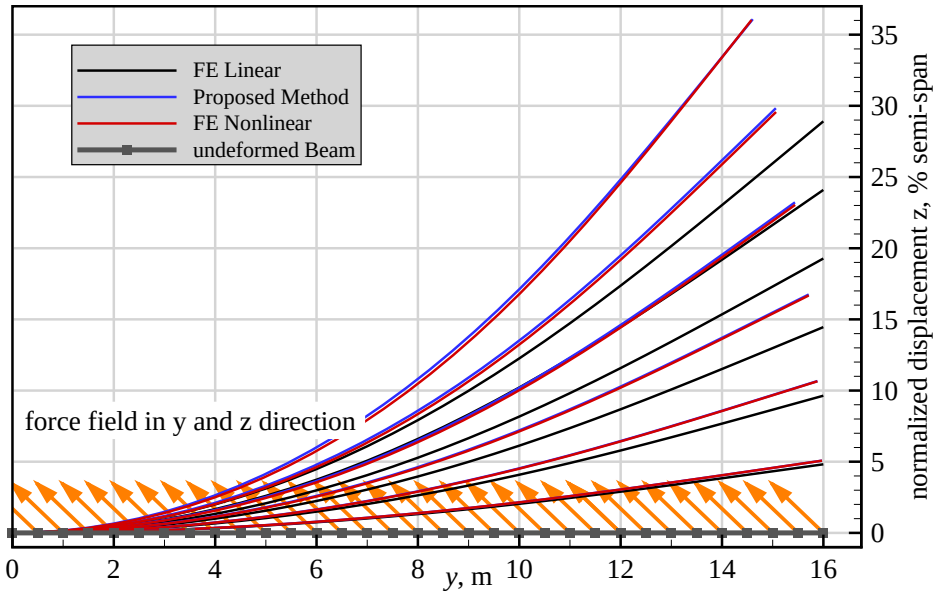

Fig. 2 Comparison of the static displacement fields for a combination of forces in the negative y and in the positive z direction applied at each node of the beam. The blue line ("Proposed Method") is the solution of the extended modal approach.

III. A Novel Approach for the Calculation of the Higher Order Mode Components

A. Basics of Displacement based, Geometrically Nonlinear Beam Theory

The method for the calculation of the higher order (quadratic, cubic, fourth-order) mode components by a series of nonlinear static FE simulations described above brings certain disadvantages with it. The scaling factors q_i must be chosen very carefully, they must be large enough to excite the nonlinearities, but not too large to ensure meaningful solutions with respect to the structural displacements. This not only requires experience in the application of the method but is also different for each new structure that is investigated. A more robust and general approach for the calculation of the higher order mode components is desirable. Ideally, they can be computed directly within a FE solver, without the need for a series of costly, nonlinear simulations. A novel approach for the computation of higher order mode components is presented in this paper. The basic idea is the successive linearization of the curvature-rotation and the curvature-displacement relationships used in nonlinear, geometrically exact beam theory. Therefore, the work of Minguet is considered, who presents a geometrically nonlinear beam theory based on Euler angles which can model arbitrary large deflections [9]. The most relevant aspects of his theory are recapped here. The deformation of the beam reference line in space is described by three displacements x, y, and z. The attitude of the cross section and the local coordinate system along the beam is defined by three Euler angles θ, β, and ψ, as illustrated in Fig. 3. First, a generalized relation between the (continuously distributed) externally applied force and moment vectors acting along the beam, which are taken as the resultants of the internal stresses and the strains (including axial strains, two transverse shear strains, the twist rate, and the two bending curvatures), is defined as follows:

$$\begin{bmatrix} F_1 \\ F_2 \\ F_3 \\ M_1 \\ M_2 \\ M_3 \end{bmatrix} = \begin{bmatrix} E_{11} & E_{12} & E_{13} & E_{14} & E_{15} & E_{16} \\ & E_{22} & E_{23} & E_{24} & E_{25} & E_{26} \\ & & E_{33} & E_{34} & E_{35} & E_{36} \\ & & & E_{44} & E_{45} & E_{46} \\ & \text{SYM} & & & E_{55} & E_{56} \\ & & & & & E_{66} \end{bmatrix} \begin{bmatrix} \epsilon \\ \gamma_{\zeta\eta} \\ \gamma_{\xi\zeta} \\ \omega_\xi \\ \omega_\eta \\ \omega_\zeta \end{bmatrix}, \tag{7}$$

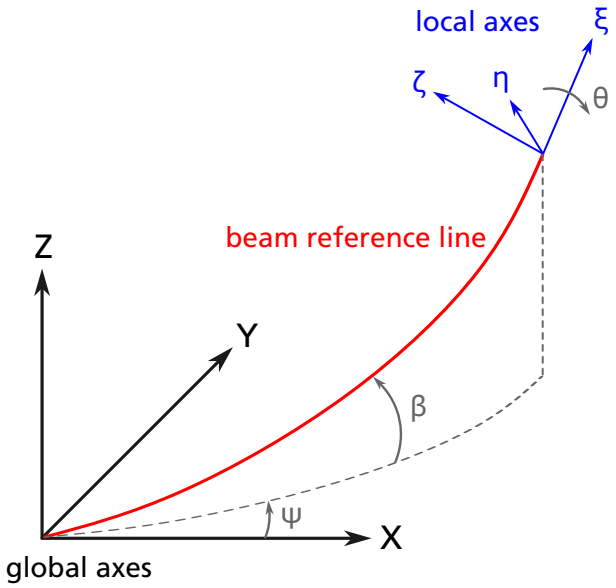

Fig. 3 Global and local frames of reference to define the position and attitude of the beam reference line and the cross section.

where E_{44} denotes the torsional stiffness, E_{55} and E_{66} denote bending stiffnesses, etc. The curvatures defined by ω are the twist rate, ω_ξ, the bending curvature about the beam's local η axis, ω_η, and the bending curvature about the beam's local ζ axis, ω_ζ. Following the calculation of the strains and curvatures, a series of coupled nonlinear, first-order compatibility differential equations is used to calculate the Euler angles ψ, β, and θ along the beam's reference line (denoted by s), which describe the rotations of the beam reference line [9]:

$$\frac{d\theta}{ds} = \omega_\xi - sin\theta\, tan\beta\, \omega_\eta - cos\theta\, tan\beta\, \omega_\zeta \quad , \tag{8}$$

$$\frac{d\beta}{ds} = -cos\theta\, \omega_\eta + sin\theta\, \omega_\zeta \quad ,$$

$$\frac{d\psi}{ds} = \frac{sin\theta}{cos\beta}\omega_\eta + \frac{cos\theta}{cos\beta}\omega_\zeta \quad .$$

It is well known that Euler angles exhibit singularities at particular angles, but the focus of this work is on "moderately" large nonlinear deflections for which it is assumed that all rotation angles along the beam stay well below ninety degrees. Once the Euler angles are computed, the displacements of the reference line of the beam with respect to the global coordinate system (denoted by x, y, and z) can be calculated by another set of first-order differential equations:

$$\frac{dx}{ds} = (1+\epsilon)\, cos\beta\, cos\psi \quad , \tag{9}$$

$$\frac{dy}{ds} = (1+\epsilon)\, cos\beta\, sin\psi \quad ,$$

$$\frac{dz}{ds} = (1+\epsilon) sin\beta \quad ,$$

where ϵ denotes the axial strain along the beam. More details about the derivation of this method are given in the paper of Minguet [9].

B. Successive Linearization of the Compatibility Equations

The next steps for the direct calculation of higher order mode components are as follows. The derivation is based on a beam model, an extension to other structural models – especially statically condensed models, which share a similar topology – is depicted subsequently.

It is assumed that the curvatures of the beam's reference line (mainly ω_ξ, ω_η, and ω_ζ) for one particular mode shape of the structure considered are available. Then the set of differential equations, Eqs.(8) can be solved to obtain the Euler angles along the beam. From the Euler angles, the displacements of the beam's reference line are obtained from the solution of Eqs.(9). For "small" strains and curvatures, the resulting displacement field would be equal to the displacement field of the particular mode. However, as the curvatures are increased, the displacements of the mode shape would appear geometrically nonlinear. This idea is illustrated by a simple example. A cantilever beam of length L with homogeneous geometrical (cross section) and material properties (Young's modulus, density) along its reference line is considered. The mode shapes (eigenvectors) and corresponding frequencies (eigenvalues) can be calculated analytically from (linear) Euler-Bernoulli beam theory; furthermore, they can be scaled to a generalized mass of unity. For the beam clamped at the left end and free at the right end, the out-of-plane mode shapes, which represent a standing wave with displacements in the z direction, are given by the following equation:

$$z(s) = 0.5\left[\left(-cos(k_n\,s) + cosh(k_n\,s)\right) + \frac{cos(k_n\,L + cosh(k_n\,L))}{sin(k_n\,L) + sinh(k_n\,L)}\left(sin(k_n\,s) - sinh(k_n\,s)\right)\right] \quad , \tag{10}$$

where k_n are the roots of the corresponding oscillation function. For the first bending mode, k_1 is approximately 1.8751 and the mode shape has the graph plotted in Fig. 4. The corresponding curvature function is obtained from the

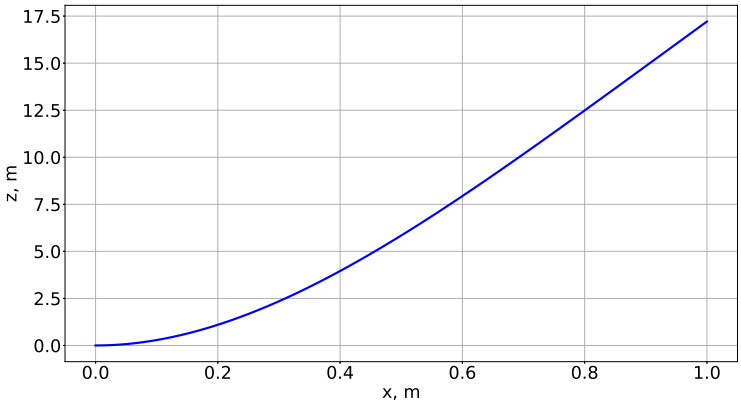

Fig. 4 First bending mode shape of an exemplary cantilever beam normalized by generalized mass of unity.

second derivative of the displacement function, Eq.(10), with respect to the beam coordinate s. For the first bending mode, the graph of the curvature is plotted in Fig. 5. The curvature of the first bending mode can be inserted into the nonlinear compatibility equations, Eqs.(8) and Eqs.(9) to obtain a "nonlinear" mode shape with geometrically large deflections, depending on the magnitude/scaling of the curvature. The nonlinear displacement field obtained from the solution of the nonlinear compatibility equations and the curvature of the first bending mode (Fig. 5) is plotted in Fig. 6, where the curvature was scaled to obtain a maximum displacement at the tip of the beam of approximately 50%. The geometrically nonlinear displacement fields are distinctive. Furthermore, it should be mentioned that the length of the beam is 1 meter – independent of the magnitude of deformation –, which means it is not "stretched" as in a linear structural analysis (as can be seen, for instance, in Fig. 2).

The higher order mode components are defined as the quadratic, cubic, and fourth-order (even more higher order terms are possible but haven't been considered so far) extensions to the linear normal modes. These terms can now be computed by successive linearization of the trigonometric functions of the differential equations Eqs.(8) and Eqs.(9).

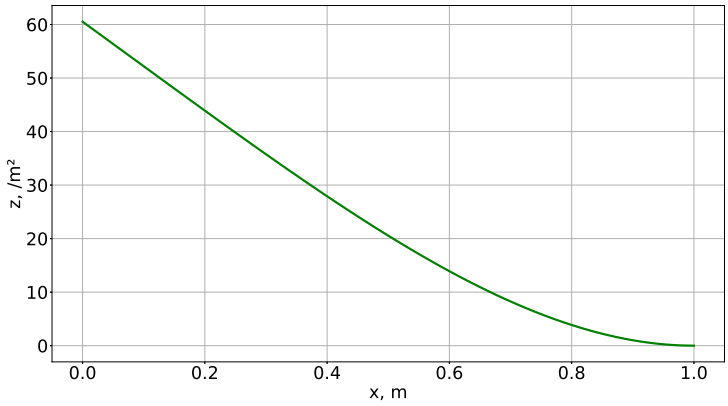

Fig. 5 Curvature of the first bending mode shape of the exemplary cantilever beam.

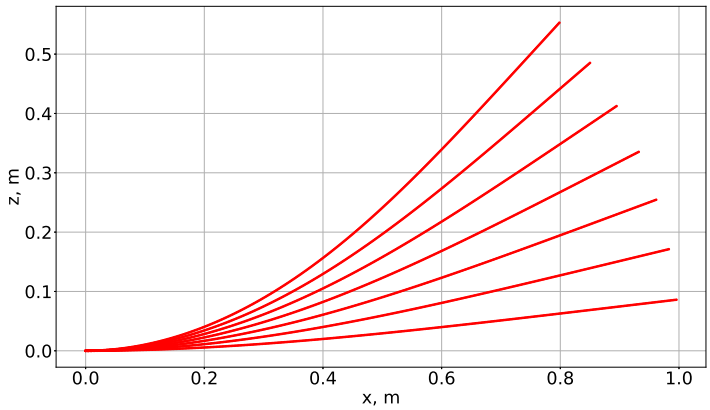

Fig. 6 Geometrically nonlinear displacement fields of the first bending mode of the cantilever beam obtained from nonlinear compatibility equations and analytic curvatures with different scaling factors.

For the cubic part, expressions with the third power of the Euler angles are retained in the coupled differential equations as follows:

$$\frac{d\theta}{ds} = \omega_\xi - (\theta - \frac{1}{6}\theta^3)\,(\beta + \frac{1}{3}\beta^3)\omega_\eta - (1 - \frac{1}{2}\theta^2)\,(\beta + \frac{1}{3}\beta^3)\omega_\zeta \quad , \tag{11}$$

$$\frac{d\beta}{ds} = -(1-\theta^2)\,\omega_\eta + (\theta - \frac{1}{6}\theta^3)\,\omega_\zeta \quad ,$$

$$\frac{d\psi}{ds} = \frac{\theta - \frac{1}{6}\theta^3}{1-\beta^2}\omega_\eta + \frac{1-\theta^2}{1-\beta^2}\omega_\zeta \quad .$$

Likewise, the quadratic approximation is given as:

$$\frac{d\theta}{ds} = \omega_\xi - \theta\,\beta\omega_\eta - (1 - \frac{1}{2}\theta^2)\,\beta\,\omega_\zeta \quad , \tag{12}$$

$$\frac{d\beta}{ds} = -(1-\theta^2)\,\omega_\eta + \theta\,\omega_\zeta \quad ,$$

$$\frac{d\psi}{ds} = \frac{\theta}{1-\beta^2}\omega_\eta + \frac{1-\theta^2}{1-\beta^2}\omega_\zeta \quad .$$

Finally, the linear approximation (which equals the corresponding expressions of the Euler-Bernoulli beam theory) is given as:

$$\frac{d\theta}{ds} = \omega_\xi \quad , \tag{13}$$
$$\frac{d\beta}{ds} = -\omega_\eta \quad ,$$
$$\frac{d\psi}{ds} = \omega_\zeta \quad .$$

A similar procedure is applied for the successive linearization of the differential equations of Eqs.(9) to obtain cubic, quadratic, and linear expressions for the computation of the global displacements of the beam's reference line as function of the Euler angles.

Staying with the simple beam example from above, the different levels of linearization can now be applied to calculate global displacements of the beam's reference line from the curvature function plotted in Fig. 5 by (numerical) integration of the differential equations. The results are shown in Fig. 7. It is remarkable that the nonlinear and cubic displacement fields are almost identical, which demonstrates that for moderately large bending deformations up to approximately 30% with respect to the length of the beam cubic approximations are typically sufficient [3]. The higher order mode components can now be extracted from these displacement fields and used in the equations of the extended modal approach, Eq.(4).

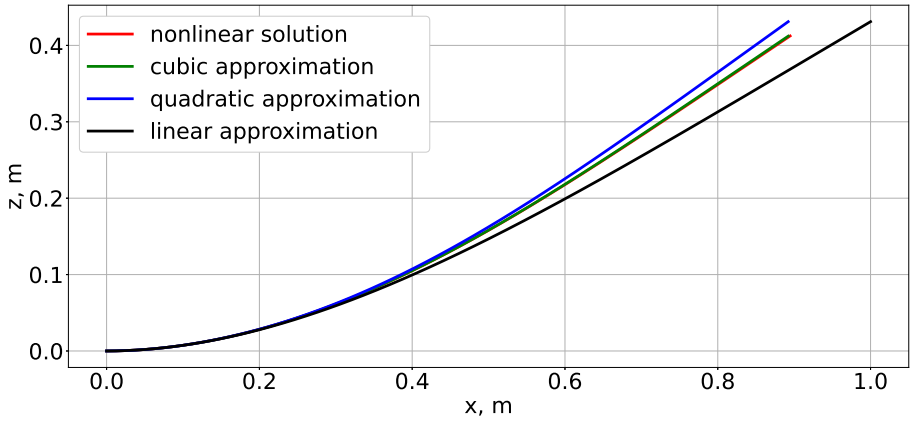

Fig. 7 Displacement fields of the first bending mode of the cantilever beam obtained from different compatibility equations (nonlinear, cubic, quadratic, and linear), according to Eqs.(8, 11, 12, and 13), which use the curvature from Fig. 5. Note that nonlinear and cubic displacement fields are almost identical.

Another important aspect should be highlighted here as well. Compared to the classical modal approach, the extended modal approach not only represents a geometrically nonlinear displacement field, but enables the coupling of individual modes (which are otherwise, i.e. in the linear case, uncoupled). This coupling can be seen in the quadratic, cubic, and fourth order mode components, as shown in Eqs.(1 and 5) and becomes important for aeroelastic applications of the extended modal approach (as an example, the combination of out of plane bending and torsion of an aircraft wing yields in plane bending deformations). Regarding the approach proposed in this work for the calculation of the higher order mode components, the coupling of the individual modes is apparent in the quadratic and cubic approximations of the compatibility equations, Eqs.(11 and 12), which remain coupled in the curvatures and the Euler angles. Only the linearized equations, Eqs.(13), are uncoupled.

C. Calculation of Mode Shape Curvature from Modal Data

An issue may arise in practical applications of the proposed approach. The curvatures of the beam reference line (or of the nodes of a condensed structural model) of the individual modes are not necessarily part of the results of a structural modal analyses with a finite element program. They can be calculated based on strain or stress results and geometric properties at particular structural locations, but the output must contain both normal and shear strains to at least calculate the twist rate ω_ξ as well as the two bending curvatures ω_η and ω_ζ. If those data are not available, they can be computed from the rotational degrees of freedom (modal rotations) of the particular mode shape by differentiation along the beam reference axis. A similar approach is applied by the Modal Rotation Method (MRM) [10]. For this work, the modal rotations are splined using a piecewise linear, interpolating spline to avoid oscillations in case the beam reference axis is kinked. A spline object is generated for each set of modal rotations and each degree of freedom (rotation about the x, y, and z axis) using the *UnivariateSpline* class of *SciPy*[1]. This class provides a method for the (analytic) calculation of derivatives of the spline, which is used to compute the curvatures of the modes.

This approach will be demonstrated for the 16m beam introduced in section II.C. Fig. 8 depicts the second out of plane (OOP) bending mode in terms of the nodal displacements in the z direction and the nodal rotations about the x axis.

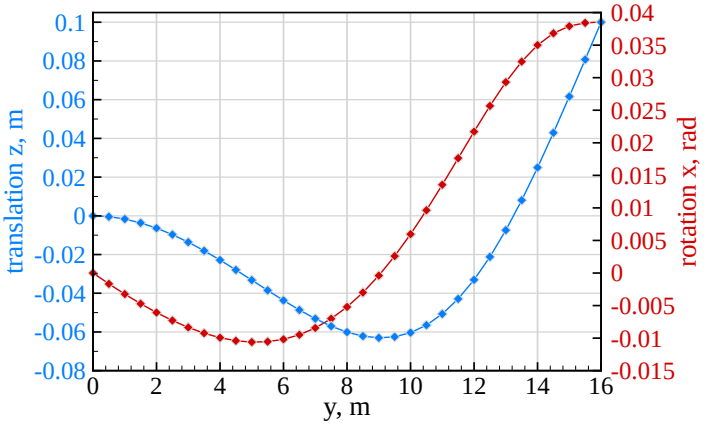

Fig. 8 Translational (z) and rotational (x) displacements of the 2nd OOP bending mode of the 16m beam.

A piecewise linear spline was used to fit the modal rotations about the x axis, its derivative is hence a function with piecewise constant values for the curvature between the FE nodes, as plotted in Fig. 9.

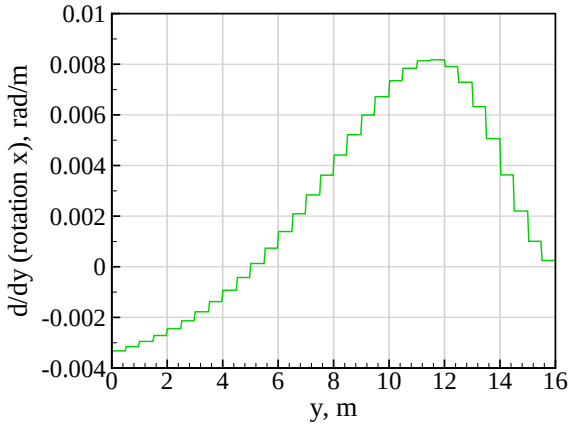

Fig. 9 Derivative of the (splined) rotational displacements of the 2nd OOP bending mode of the 16m beam.

[1] https://scipy.org

IV. Numerical Studies

In this section the proposed method will be applied for the calculation of the linear and higher order mode components of the 16m beam and a (statically) condensed model of a generic, slender composite wingbox. The focus is on the comparison of the mode components, applications of the extended modal approach with these structures have been presented in earlier works of the author.

A. Calculation of Higher Order Mode Components for the 16m Beam

The first application of the approach is for the 16m beam, for which higher order mode components (quadratic and cubic) will be computed and plotted. A numerical integration procedure is used to calculate the linear, quadratic, and cubic mode components of the corresponding (linearized) compatibility differential equations, Eqs. 13, 12, and 11 together with the corresponding (linearized) equations that relate the displacements to the Euler angles, Eq. 9. The numerical integration is done with the *solve_ivp* function from the *scipy.integrate* package. This method numerically integrates a system of ordinary differential equations given a vector of initial values. The integration starts at the clamped end, where the Euler angles and displacements for all modes are zero. The curvatures of the modes were calculated using the approach described in section III.C. Fig. 10 shows the linear, quadratic, and cubic mode components of the first OOP bending mode of the 16m beam. The linear mode component, which is obtained from the integration of Eq. 13, is comparable to the normal mode computed by an eigenvalue analyses with MSC Nastran SOL103. Note the quadratic mode component has values in the (negative) y direction only. Furthermore, the magnitude of the cubic mode component is very low, but it must be noted that this component is scaled with the third power of the generalized coordinate for the calculation of the nodal displacement field (Eq. 5).

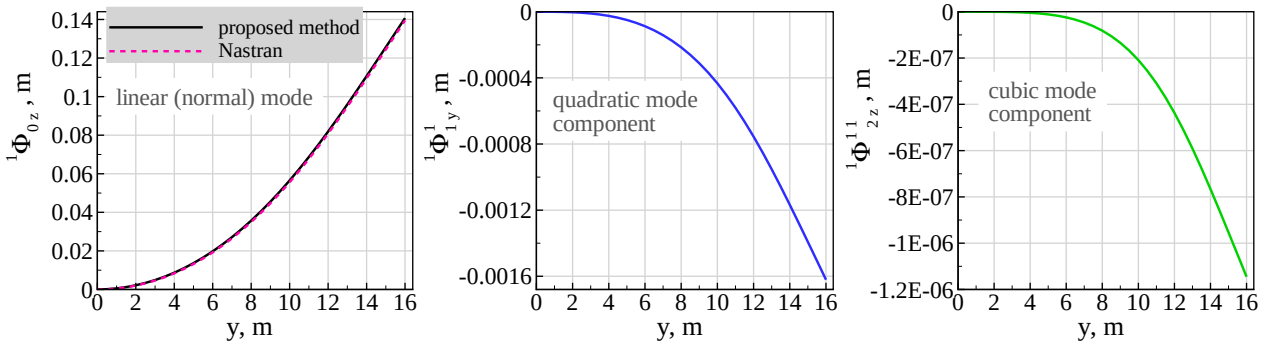

Fig. 10 Linear, quadratic, and cubic mode components for the 1st OOP bending mode of the 16m beam. Linear mode component is comparable to normal mode solution from MSC Nastran SOL103. Note the quadratic mode component is a (negative) displacement in the y direction.

As a simple demonstration, the different mode components are now used to calculate corresponding physical (nodal) displacement fields of the first and the second bending mode by application of Eq. 5. The generalized coordinate was chosen to yield tip deflections large enough to highlight nonlinear effects. Nonlinear displacement fields, which were obtained from the solution of Eqs. 8 and 9 are added as reference. The displacement fields of the first bending mode are plotted in Fig. 11. Only the z component is plotted because there is no displacement in the x direction. For deformations up to approximately 15%, the linear mode together with the quadratic mode component yield a very good approximation of the displacement field when compared to the nonlinear solution. For displacements greater than approximately 25%, the cubic mode component should be added. The displacement fields of the second bending mode are plotted in Fig. 12. As for the first bending mode, adding the quadratic mode component yields a very good approximation of the displacement field for moderately large deformations. It must be mentioned that the contribution of the second bending mode to the overall displacement field is much less pronounced than the contribution of the first bending mode for typical aircraft (wing) applications even in states of large deformations.

B. Calculation of Higher Order Mode Components for a Composite Wingbox

Of course the question regarding the usefulness of this entire approach arises. A number of nonlinear beam theories are available which can be used for the calculation of structures with geometrically large deformations [11–17]. The intention of this work is a different one. During the preliminary design of aircraft, one of the main tasks is structural

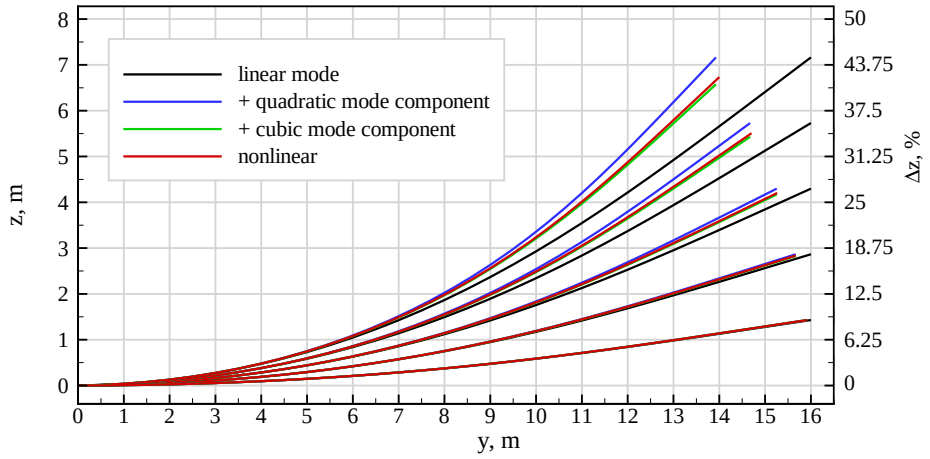

Fig. 11 Displacement fields from linear, quadratic, and cubic mode components for the 1st OOP bending mode of the 16m beam computed with Eq. 5. The generalized coordinate is scaled from -5 to -25 in steps of -5. Nonlinear result (red line) corresponds to the solution of Eqs. 8 and 9.

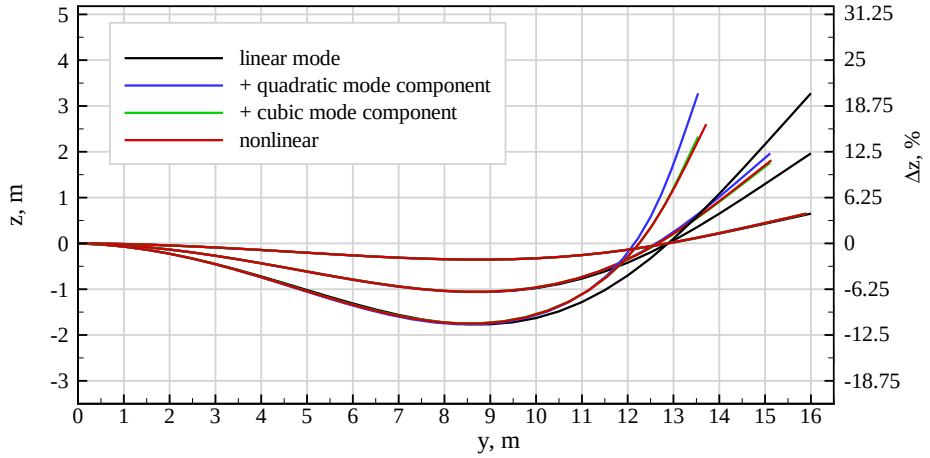

Fig. 12 Displacement fields from linear, quadratic, and cubic mode components for the 2nd OOP bending mode of the 16m beam computed with Eq. 5. The generalized coordinates are [-2, -6, -10]. Nonlinear result (red line) corresponds to the solution of Eqs. 8 and 9.

optimization. A detailed finite element model of the aircraft is used for this, and the goal is to find an optimum regarding minimum mass of the primary (load carrying) structure subject to a number of load cases and constraints. The global finite element model is build from shell and beam elements which represent the skins, spars, ribs, stringers, etc. The thicknesses of the components or particular lamination parameters are typically used as design variables. During the optimization process, the stiffness and mass properties of the structure change, which in turn requires new computations of loads to account for updates of the model. These loads analyses are typically based on condensed structural models, which use a Guyan reduction (static condensation) to significantly reduce the number of degrees of freedom and thus simplify the maneuver and gust loads analyses [18]. The DLR in-house structural optimization process is detailed in the work of Schulze and Co-authors [19–21].

With the current trend in jet transport aircraft design towards high aspect ratio, slender wings, the flexibility of these structures is increased significantly and (geometrical) nonlinearities due to large deflections are to be expected in the loads analyses and structural optimization stages in aircraft design. As mentioned above, a geometrical nonlinear beam theory could be applied for this purpose. However, this requires the computation of the cross section properties of the detailed finite element model along the span of the wing (moments of inertia for bending and mass, etc.) which

is needed for any beam theory. Tools to calculate cross section data from (complex) finite element models are available, but the application can be complex. A simpler approach would be to use the condensed model. The idea is to run a normal modes analyses with the condensed model and to compute the curvatures of the individual modes using the approach described in section III.C. These curvatures can then be used with the method proposed in this work to obtain the higher order mode components which enables the application of the extended modal approach in a nonlinear loads analysis within the structural optimization loops. An application of this process to a high aspect ratio, composite wingbox is demonstrated in the following.

This test case consists of a 20-m span, generic wingbox configuration with a sweep angle of 1.8 degrees composed of quadrilateral shell elements [2]. This three-dimensional wingbox resembles a real aircraft wing much more realistically and is built from spars, ribs, as well as upper and lower skins. Anisotropic materials (CFRP) are used for all elements of the wing by means of MSC Nastran *MAT2* cards. Furthermore, the thicknesses of the shell elements are reduced along the wingspan to obtain even curvature in bending deformation for typical aerodynamic loadings. No additional discrete mass elements were used for this test case. The model contains 1950 nodes, 2005 elements, and 254 different anisotropic materials. The outer shape of the wingbox is defined by a NACA 4415 airfoil at the root of the wing and a NACA4412 airfoil at the tip of the wing; the FE model is illustrated in Fig. 13. The mode shapes of the full FE model

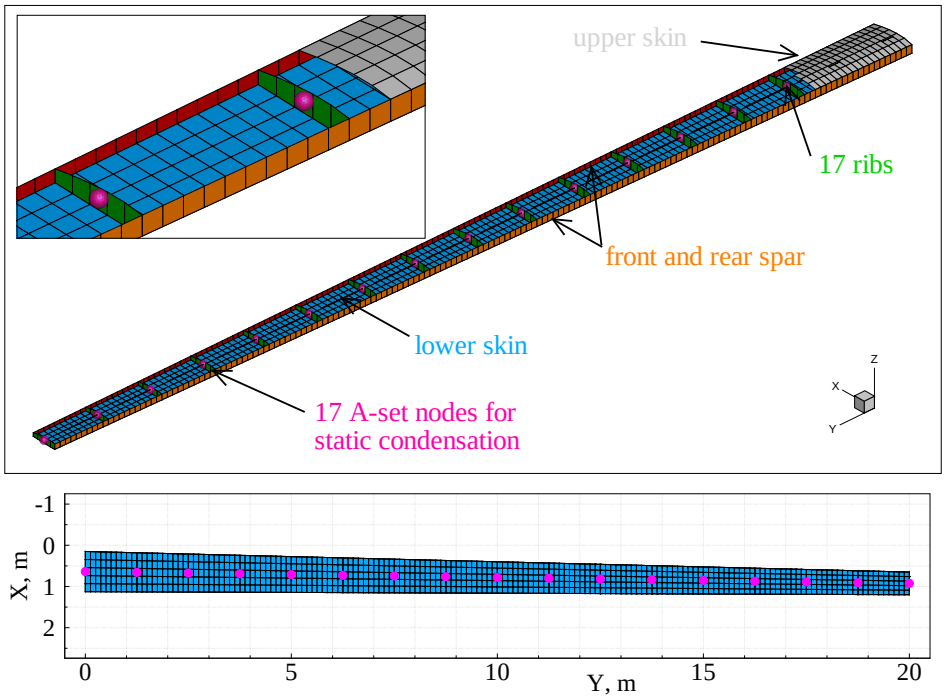

Fig. 13 Layout of the high aspect ratio, 20m half span wingbox with CFRP shell elements and (A-set) nodes for static condensation.

are plotted in Fig. 14. A static condensation (Guyan reduction) was used within MSC Nastran to obtain the normal modes on the reduced set (A-set nodes in Fig. 13). For the proposed method, the modal rotations of these nodes were used for the approach described in section III.C to calculate the curvatures of the individual modes. For the first out of plane bending mode (upper left plot in Fig. 14) the curvatures are plotted in Fig. 15. As for the 16m beam example (cf. Fig. 9), the curvatures obtained by this approach are piecewise constant due to the splining of the modal rotations, which use piecewise linear functions.

Because the composite wingbox is a slender, high aspect ratio structural component, its low frequency mode shapes are similar to that of a beam model. Thus the individual mode components are not plotted here, they are qualitatively comparable to the ones of the 16m beam (Fig. 10).

The linear and higher order mode components can now be computed with the approach described in section III.B. Physical displacement fields are plotted in Figs. 16 and 17 for the first and the second OOP bending mode of the wingbox model (these are the first and third mode plot in the upper row of Fig. 14). The displacements in both the x and the z

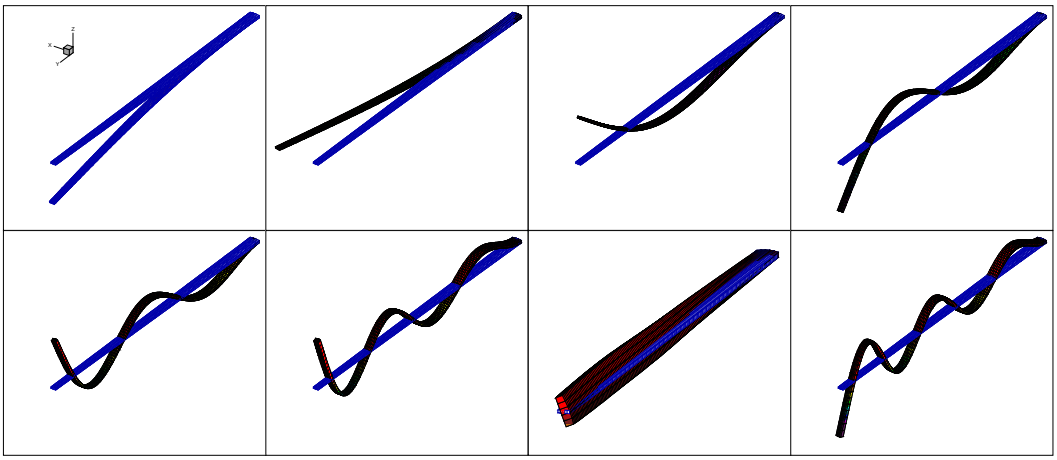

Fig. 14 The eight lowest normal mode shapes of the full FEM of the wing box test case computed by an eigenvalue analysis with MSC Nastran SOL103.

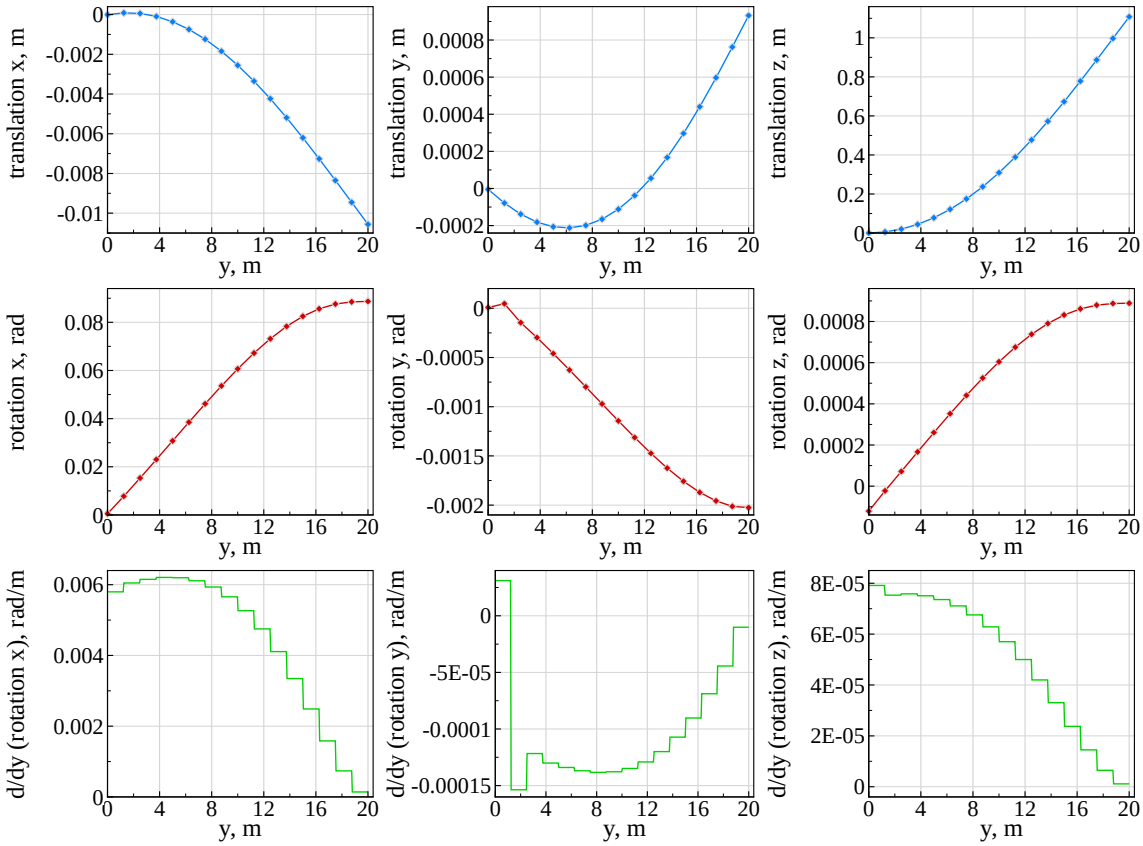

Fig. 15 Translational and rotational displacements of the A-set nodes for the 1st OOP bending mode of the wing box test case (upper two rows). Derivatives of the (splined) rotational displacements (bottom row).

direction are shown. Even though the deformations in the x direction are very small for these two modes, the differences between the displacements computed using only the linear mode component and the others are significant (especially for the second bending mode). Adding the quadratic mode component already yields a significant improvement compared to the linear mode. The differences (for the displacements in the x direction) between the results using the quadratic

and the cubic mode components to the nonlinear reference are less pronounced. A similar behavior to the 16m beam test case is obtained for the displacements in the z direction. For aeroelastic analyses, these deformation fields are the most important ones, and the accuracy gained by adding the quadratic and cubic mode components to the linear modes is reflected very well in the two plots on the right of Figs. 16 and 17.

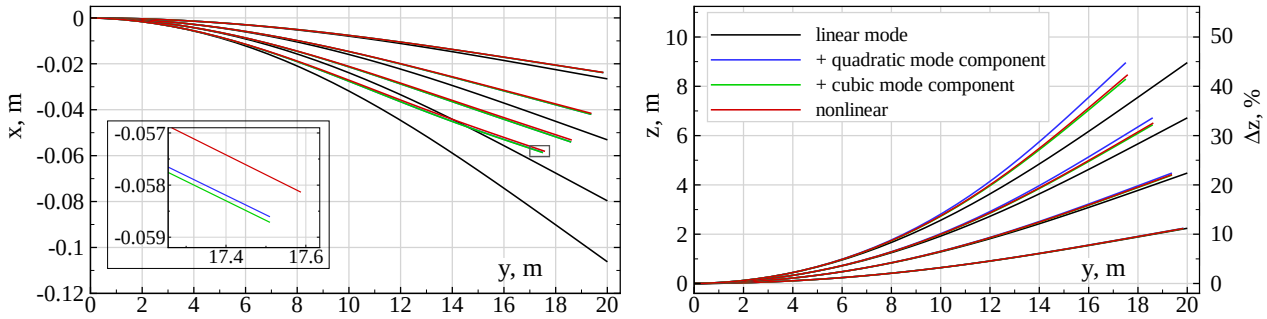

Fig. 16 Displacement fields from linear, quadratic, and cubic mode components for the 1st OOP bending mode of the composite wingbox computed with Eq. 5. The generalized coordinate is scaled from -10 to -40 in steps of -10. Nonlinear result (red line) corresponds to the solution of Eqs. 8 and 9.

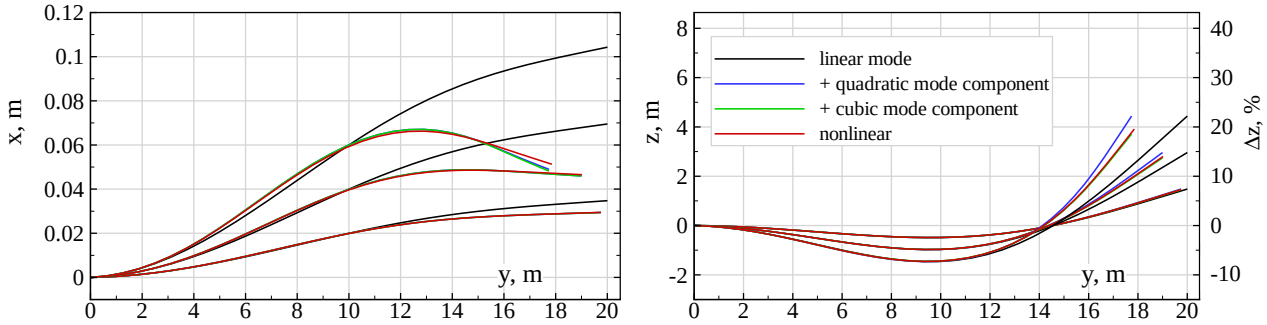

Fig. 17 Displacement fields from linear, quadratic, and cubic mode components for the 2nd OOP bending mode of the composite wingbox computed with Eq. 5. The generalized coordinate is scaled from 5 to 15 in steps of 5. Nonlinear result (red line) corresponds to the solution of Eqs. 8 and 9.

V. Conclusion and Outlook

The extended modal approach is an elegant method for the geometrically nonlinear analyses of highly flexible aircraft structures. It is based on the extension of the classical modal approach by higher order mode components which represent a geometrically nonlinear displacement field and can be used for tip deflections up to approximately 30%. So far, its practical applications were difficult because of the efforts needed to calculate the higher order mode components. A new method to circumvent these difficulties is presented in this work. Assuming a complex, detailed finite element model of an aircraft structure can be reduced to a subset of structural nodes using static condensation (Guyan reduction). Rotational degrees of freedom of the eigenvectors (modal rotations) are splined and differentiated along a reference line to compute the corresponding curvatures. These curvatures are then used in successively linearized compatibility equations (derived from the displacement based, geometrically nonlinear beam theory) to calculate the higher order mode components of the structure. Two test cases are presented that highlight the ability to represent geometrically nonlinear displacement fields of individual modes and the simplicity of this approach. Compared to the geometrically nonlinear beam theory, the process as a whole can be seen as a method that avoids the integration of the nonlinear compatibility equations, Eqs. 8 and 9, by "pre-integrating" them to a set of higher order mode components which are then used with the extended modal approach.

Further research will be carried out to make the proposed method applicable to more complex (condensed) structural models. Especially the case with structural components (wing, fuselage) that share a common point (e.g. in the center of the fuselage at the wing attachment or the empennage) and extend to different sides need a partition of the integration process along the different components with a proper alignment of the boundary conditions (same DOFs of the eigenvectors and higher order mode components at the intersecting nodes). Also a formulation to account for nonlinear load displacement relationships must be developed. This is partially included in the quadratic mode components, which become part of the linear stiffness term (cf. Eq. 4), but it must be verified that the method can model the migration of eigenvalues in geometrically large deflections, which can become significant for particular structural models [22].

References

[1] Ritter, M., Cesnik, C. E. S., and Krüger, W. R., *An Enhanced Modal Approach for Large Deformation Modeling of Wing-Like Structures*, 56th AIAA/ASCE/AHS/ASC Structures, Structural Dynamics, and Materials Conference, Kissimmee, Florida, Jan 2015.

[2] Ritter, M. and Cesnik, C. E. S., *Large Deformation Modeling of a Beam Type Structure and a 3D Wingbox using an Enhanced Modal Approach*, 57th AIAA/ASCE/AHS/ASC Structures, Structural Dynamics, and Materials Conference, San Diego, California, Jan 2016.

[3] Ritter, M. R., *An Extended Modal Approach for Nonlinear Aeroelastic Simulations of Highly Flexible Aircraft Structures*, Dissertation, Technische Universität Berlin, 2019.

[4] Medeiros, R. R., Cesnik, C. E. S., and Coetzee, E. B., "Computational Aeroelasticity Using Modal-Based Structural Nonlinear Analysis," *AIAA Journal*, Vol. 58, No. 1, 2020, pp. 362–371.

[5] Segalman, D. J. and Dohrmann, C. R., "A Method for Calculating the Dynamics of Rotating Flexible Structures, Part 1: Derivation," *Journal of Vibration and Acoustics*, Vol. 118, No. 3, Jul 1996, pp. 313–317.

[6] van Zyl, L. H., Sutherland, A. N., and Rossouw, P. S., *Parabolic Mode Shapes: What they are, where to get them and what to do with them*, International Forum on Aeroelasticity and Structural Dynamics, Seattle, Washington, 2009.

[7] van Zyl, L. H. and Mathews, E. H., "Quadratic Mode Shape Components From Linear Finite Element Analysis," *ASME Journal of Vibration and Acoustics*, Vol. 134, Feb. 2012.

[8] Mignolet, M. P., Przekop, A., Rizzi, S. A., and Spottswood, S. M., "A review of indirect/non-intrusive reduced order modeling of nonlinear geometric structures," *Journal of Sound and Vibration*, Vol. 332, No. 10, 2013, pp. 2437 – 2460.

[9] Minguet, P. and Dugundji, J., "Experiments and analysis for composite blades under large deflections. I - Static behavior," *AIAA Journal*, Vol. 28, No. 9, 1990, pp. 1573–1579.

[10] Drachinsky, A. and Raveh, D. E., "Modal Rotations: A Modal-Based Method for Large Structural Deformations of Slender Bodies," *AIAA Journal*, Vol. 58, No. 7, 2020, pp. 3159–3173.

[11] Cesnik, C. and Su, W., chap. Nonlinear Aeroelastic Modeling and Analysis of Fully Flexible Aircraft, Structures, Structural Dynamics, and Materials and Co-located Conferences, American Institute of Aeronautics and Astronautics, Apr 2005.

[12] Su, W. and S. Cesnik, C. E., "Dynamic Response of Highly Flexible Flying Wings," *AIAA Journal*, Vol. 49, No. 2, Feb 2011, pp. 324–339.

[13] Shearer, C. M. and Cesnik, C. E., "Nonlinear Flight Dynamics of Very Flexible Aircraft," *Journal of Aircraft*, Vol. 44, No. 5, Sep 2007, pp. 1528–1545.

[14] Cesnik, C. E. S., Palacios, R., and Reichenbach, E. Y., "Reexamined Structural Design Procedures for Very Flexible Aircraft," *Journal of Aircraft*, Vol. 51, No. 5, 2014, pp. 1580–1591.

[15] Su, W. and Cesnik, C. E. S., "Strain-Based Analysis for Geometrically Nonlinear Beams: A Modal Approach," 53^{rd} AIAA/ASME/ASCE/AHS/ASC Structures, Structural Dynamics and Materials Conference, Honolulu, Hawaii, April 2013.

[16] Goizueta, N., Drachinsky, A., Wynn, A., Raveh, D., and Palacios, R., "Flutter Predictions for Very Flexible Wing Wind Tunnel Test," *AIAA Scitech 2021 Forum*, Virtual Conference, Jan 2021.

[17] del Carre, A., Muñoz-Simón, A., Goizueta, N., and Palacios, R., "SHARPy: A dynamic aeroelastic simulation toolbox for very flexible aircraft and wind turbines," *Journal of Open Source Software*, Vol. 4, No. 44, Dec. 2019.

[18] Guyan, R. J., "Reduction of stiffness and mass matrices," *AIAA Journal*, Vol. 3, No. 2, 1965, pp. 380–380.

[19] Schulze, M., Neumann, J., and Klimmek, T., "Parametric Modeling of a Long-Range Aircraft under Consideration of Engine-Wing Integration," *Multidisciplinary Digital Publishing Institute MDPI, Aerospace, Special Issue "Aeroelasticity, Volume II"*, Vol. 8, No. 1, December 2020, pp. 1–20.

[20] Klimmek, T., Schulze, M., Abu-Zurayk, M., Ilic, C., and Merle, A., *cpacs-MONA – An independent and in high fidelity based MDO tasks integrated process for the structural and aeroelastic design for aircraft configurations*, International Forum on Aeroelasticity and Structural Dynamics IFASD, Savannah, Georgia, June 2019.

[21] Ritter, M. R., Fehrs, M., and Schmalz, M., *Preliminary Structural Design of a High Aspect Ratio Transport Aircraft With Laminar Wing*, 34th Congress of the International Council of the Aeronautical Sciences ICAS, Florence, Italy, Sep 2024.

[22] Ritter, M. R., Hilger, J., Ribeiro, A. F. P., Öngüt, E., Righi, M., Riso, C., Cesnik, C. E. S., dos Santos, L. G. P., Raveh, D., Drachinsky, A., Stanford, B., Chwalowski, P., Kovvali, R. K., Singh, B., Düssler, S., Cheng, K. C. W., Palacios, R., Santos, J. P. T. P., Marques Jr., F. D., Begnini, G. R., Verri, A. A., Lima, J. F. B. O., de Melo, F. B. C., and Bussamra, F. L. S., *Collaborative Pazy Wing Analyses for the Third Aeroelastic Prediction Workshop*, AIAA Scitech 2024 Forum, Orlando, Florida, January 2024.